PROCEEDINGS OF SCIENCE

The road to a time-resolved RICH at LHCb

Federica Borgato on behalf of the LHCb RICH collaboration[a,b,*]

[a] *Dipartimento di Fisica dell'Università di Padova, Padova, Italy*

[b] *INFN, Sezione di Padova, Padova, Italy*

E-mail: federica.borgato@cern.ch

The LHCb Collaboration is planning a major "Upgrade II" of the experiment with the purpose to increase the instantaneous luminosity by a factor of 5 to 1.5x10^{34}cm^{-2}s^{-1} during Long Shutdown 4 of the LHC. This poses stringent requirements on the capabilities of subdetectors due to the increased particle multiplicity and detector occupancy. The Upgrade II LHCb RICH (Ring-imaging Cherenkov) subsystem will require improvements in spatial and time resolution to maintain good particle identification performance in this environment. To address these challenges, an improvement in the readout electronics is planned during the Long Shutdown 3 (LS3), from 2026 to 2028. The goal is to timestamp the data with an accuracy better than O(100) ps from Run4 (2029-2032) onwards, in parallel with the development of novel sensors capable of sub-100 ps time resolution for Run5 (2035-2038). The LS3 enhancements foresee the use of the FastRICH, a 65-nm CMOS front-end readout chip, under development by CERN and ICCUB. In these proceedings a prototype opto-electronic chain for Cherenkov photon detection with precise-timing is presented as a proof-of-principle for the future RICH detectors. This readout chain is equipped with the FastIC, a precursor to the FastRICH with a similar dynamic range. In order to evaluate the time resolution of the prototype photo-detection chain equipped with the FastIC chip, beam test campaigns were conducted in 2021 and 2022 at CERN SPS charged particle beam facility with 180 GeV/c protons and pions. The results of such beam tests are presented, with a focus on the final results coming from the timing analysis and on the corrections applied to account for the time-walk effect.

The European Physical Society Conference on High Energy Physics (EPS-HEP2023)
21-25 August 2023
Hamburg, Germany

*Speaker

1. Introduction

The LHCb detector will undergo a major upgrade in Long Shutdown 4 during the high luminosity phase of LHC and having detectors with timing capabilities will be fundamental in order to mitigate the multiple proton-proton interactions per bunch crossing. In particular, concerning the LHCb RICH detector, the increased occupancy would cause a degradation of the Particle Identification (PID) performance. In this context the LHCb RICH collaboration is conducting an R&D in order to develop a prototype single-photon detector with precise-timing capabilities within the testbeam framework described in [1].

2. The LHCb RICH detector

The LHCb experiment relies on the RICH detector system for the charged hadron identification in a wide momentum range. The RICH system is composed of two distinct RICH detectors. The first, known as RICH1, is positioned upstream of the LHCb magnet and uses C_4F_{10} as gas radiator to identify particles with momenta ranging from ≈2.6 to ≈65 GeV/c. The second detector, RICH2, is situated downstream of the magnet and employs a CF_4 gas radiator, allowing for precise identification of hadrons within a momentum range spanning from ≈15 to ≈100 GeV/c. Cherenkov photons, generated within the gas radiators, are efficiently directed towards an array of Multianode Photomultipliers (MAPMT) by a spherical mirror followed by a planar one.

3. Exploiting the timing information with the RICH detector

It has been demonstrated [2] that when considering a specific particle trajectory with known momentum, it is feasible to forecast the time of arrival (ToA) of Cherenkov photons on the detector plane with a precision better than 10 ps. Exploiting such precise-timing information for background and noise rejection would allow to improve the RICH PID performance. In order to achieve this without increasing the data volume by orders of magnitude, a readout electronics capable of a nanosecond-scale time shutter around the expected RICH detector hit time and a time gate in the reconstruction software is being considered. The nanosecond-scale time gate reduces the TDC range and eliminates out-of-time background hits from particle interactions with the photon sensors and beam. Such a gate is already applied for the Run3 LHCb RICH at lower resolution. The further step will be to develop electronics endowed with a TDC with bins smaller than the sensor time resolution, in order to consider only photons within a time gate around the predicted hit times from photons emitted by the partcle applied in software. The LHCb RICH LS3 enhancements aim to equip the detector with new front-end readout electronics including the FastRICH ASIC capable of time-stamping photon detector hits with ≈25 ps time bins [3]. There is no plan to change the current photon sensors, the Hamamatsu MAPMTs, which have a time resolution of ≈ 150 ps.

4. The beam test campaign at CERN-SPS

The goal of the beam test campaign was to test a prototype readout chain equipped with the FastIC [4], the predecessor of the FastRICH, for precise-timing of the detected Cherenkov photons.

The beam test setup involved a borosilicate glass lens placed upstream of the sensors, to generate Cherenkov photons and focus the Cherenkov ring on the detector plane. The sensors used in the tests included the 1-inch and 2-inch MAPMTs[1] currently used in the LHCb RICH, as well as a Silicon Photomultiplier matrix[2]. Each sensor was accompanied by a dedicated front-end board and

[1]Hamamatsu Photonics, R11265-103-M64 and R12699-406-M64 datasheets.

[2]Hamamatsu Photonics, S14161-3050HS-08 datasheet.

a digital board (DB) for signal extraction. The DB incorporated a custom Time-to-Digital Converter implemented in an FPGA with an average bin width of 150 ps [5]. The trigger for the setup was provided by a crossed pair of scintillators combined with a Micro-Channel Plate Photomultiplier (MCP-PMT), which served as the time reference for the system.

The focus of this analysis will be on the results concerning the 1-inch MAPMT. Various configurations have been considered, both changing the focus of the Cherenkov light ring and the MAPMT high voltage conditions. Figure 1 displays the hitmaps for the three different datasets that have been analyzed.

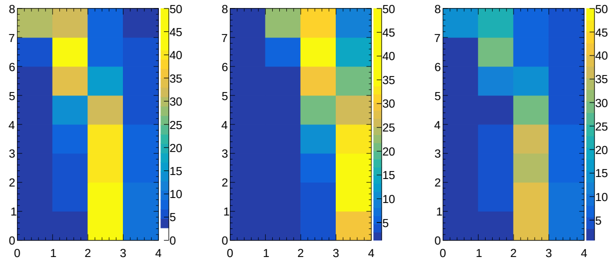

Figure 1: MAPMT hitmaps for the focused ring configuration HV=-1000V, the defocused ring configuration HV=-1000V and the focused ring configuration HV=900V. The occupancy is expressed as the percentage of channels fired on for each trigger event.

5. Single-photon time resolution: analysis method

The TDC-in-FPGA system records the ToA and falling edge of the photon signal for all 32 channels of the MAPMT read out by the FastIC, in addition to capturing the ToA of the reference signal from the MCP-PMT. The TDC time window starts at the rising edge of the 25 ns clock when a trigger event is recorded. The recorded ToA of the MCP-PMT signal, measured in TDC bins, is shown in Figure 2. The distribution is uniform as the particle arrival is asynchronous with the system clock. Figure 3 illustrates a similar spread in asynchronous ToA for single-photon events on a typical Cherenkov ring MAPMT channel. However, since both the MCP-PMT and MAPMT signals originate from the same track events, the distribution of the time difference, denoted as Δ ToA (Channel$_{\mathrm{MAPMT}}$-MCP) and shown in Figure 4, is narrower. This narrower distribution enables the extraction of the single-photon time resolution (SPTR). In the following, the analysis method will be described for a single MAPMT channel.

In this analysis, the data are grouped in subsets to eliminate two primary factors influencing time resolution: time walk and TDC-bin variation. Time walk is a consequence of the fluctuations

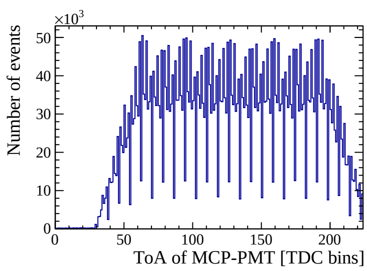

Figure 2: Recorded ToA distribution of the MCP-PMT with respect to the start of the TDC readout window.

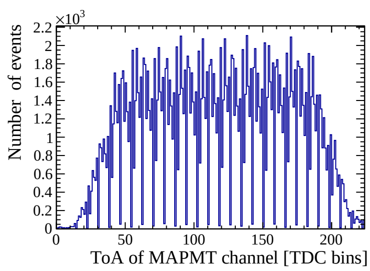

Figure 3: Recorded ToA distribution of a typical MAPMT channel with respect to the start of the TDC readout window.

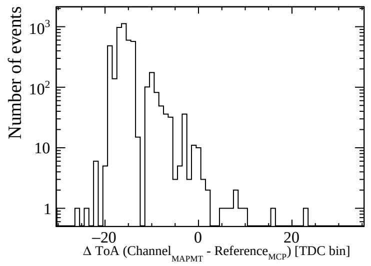

Figure 4: The time difference distribution of a 1-inch MAPMT channel with respect to the MCP-PMT, in units of TDC bins. These data are a subset for one MCP-PMT ToA bin.

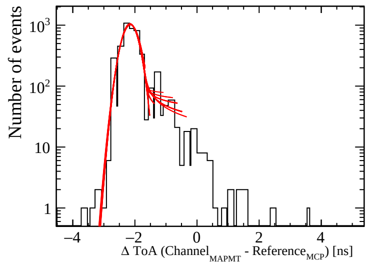

Figure 5: The same distribution as in Figure 4, using the calibration data to convert to nanoseconds for the MAPMT TDC bins and the single MCP-PMT reference bin. Moreover the CrystalBall fits to the distribution are displayed, with different fit ranges in order to estimate the systematic uncertainty on the Gaussian sigma parameter.

in MAPMT signal amplitudes. At a fixed threshold, this phenomenon results in earlier ToA for large signals and delayed ToA for signals near the threshold. To disentangle this effect from the SPTR, the data is partitioned into subsets based on Time-over-Threshold (ToT) bins. Within a given ToT bin, time walk is minimal since the signals exhibit nearly identical pulse shapes. The variation in TDC bin width affects both the reference time from the MCP-PMT and the MAPMT channel being analyzed. To regroup events with similar TDC uncertainty in the reference time, the data is categorized based on the ToA bin of the MCP-PMT. The TDC has a periodic structure, as it is possible to observe in Figure 2, by which in total there are 14 sets of 16 repeated bins. The data were therefore subdivided into 16 groups by accumulating these repeated bins.

The data pertaining to a specific group of MCP-PMT TDC bins is presented in Figure 4, and it is expressed in terms of TDC bins. A pattern emerges within the data due to the variable width of TDC bins. Narrower TDC bins exhibit lower event counts compared to broader TDC bins. In Figure 5, this effect is rectified through the conversion of the data from TDC bins to picoseconds, achieved via TDC calibration. The time associated with each bin is computed by summing the widths of all preceding bins and adding half of the width in picoseconds of the bin in question. The histogram depicted in Figure 5 employs variable bin widths that mirror the TDC bin width.

The time difference distributions, of which Figure 5 is an example, are fitted using the CrystalBall function, with the time resolution derived from the Gaussian sigma parameter. Multiple fits are performed, adjusting the fitting range to account for parameter variations. A subset of Gaussian sigmas is isolated by selecting fits which well describe the distribution, as one can observe in Figure 5. Subsequently, the simple mean and standard deviation of this subset are computed. In order to find a representative time resolution for this subset out of the many fits performed (as in Figure 5), the Gaussian sigma which is the closest to the subset mean is taken. Such reference time resolution is denoted as $\hat{\sigma}_t^{bin}$, with "bin" referring to a previously defined subset of individual MCP-PMT ToA bins. The associated uncertainty is computed as the quadratic sum of the fitting uncertainty and the standard deviation of the subset. For each MCP-PMT ToA bin, the time resolution is estimated by subtracting the MCP-PMT TDC bin width contribution:

$$\sigma_t^{bin} = \sqrt{(\hat{\sigma}_t^{bin})^2 - (\sigma_t^{MCPbin})^2} \tag{1}$$

where σ_t^{MCPbin} is obtained by dividing the MCP-PMT ToA bin width of the specific subset by $\sqrt{12}$. The uncertainty associated with σ_t^{bin}, denoted as $\sigma_{\sigma_t^{bin}}$, is determined by combining, in quadrature, the statistical component arising from fit uncertainty and the systematic component derived from the standard deviation of the set of successful fits.

Subsequently, starting from these fitted subsets, the time resolutions are recombined in the following two stages to obtain the SPTR:

- The 16 obtained values of σ_t^{bin} from the MCP-PMT ToA groups are recombined using a weighted average, in order to obtain the time resolution for each subset of a single ToT bin, $\sigma_{t,singleToT}$.

  To account for uncertainty underestimations, the reduced χ^2 of each σ_t^{bin} with respect to the weighted average, $\sigma_{t,singleToT}$, is computed. If such reduced χ^2 is higher than 1, the uncertainty on σ_t^{bin} is weighted accordingly [6].
- In Figure 6, the time resolution of a typical MAPMT channel with respect to the MCP-PMT is reported as a function of the MAPMT ToT bin number. A ToT range of ±3 bins around the most populated bin was chosen. In order to combine the time resolutions from these ToT bins, each $\sigma_{t,singleToT}$ was summed quadratically, weighted by its statistics.

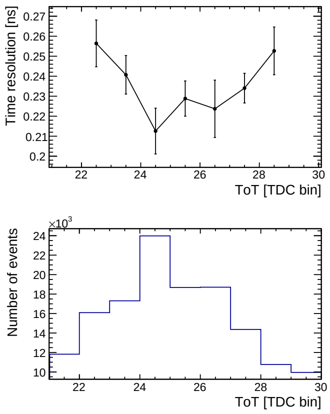

Figure 6: 1-inch MAPMT channel time resolution with respect to the MCP-PMT reference time, plotted as a function of the MAPMT ToT in units of TDC bins.

6. Single-photon time resolution results

Figure 7 displays the time resolution obtained for the channels on the Cherenkov ring as a function of the channel number. Only the results for such channels are displayed since those are the ones that contain suitable statistics for analysis. Each time resolution result has been respectively corrected for the different jitter contributions, namely the $\sigma_{\text{MCP-PMT}} \approx 110$ ps, $\sigma_{\text{FastIC}} \approx 25$ ps and $\sigma_{\text{TDC bins}} \approx 150/\sqrt{12}$ ps. To obtain an overall time resolution, the simple mean and standard deviation of such set of data is computed. Table 1 reports the results for two configurations: including and excluding the channels which are located at the border of the MAPMT. Such channels showed a worse time resolution with respect to the others and require additional investigation..

In the case of the focused Cherenkov ring, high voltage equal to -1000V, the time resolution obtained excluding the border channels is found out to be compatible with the expected MAPMT Transit Time Spread of approximately 150 ps from the manufacturer. Comparing the focused and defocused Cherenkov ring data set, it is possible to notice that in the defocused case the time resolution estimation is higher, yet still compatible with the one of the focused case. The data set with focused Cherenkov ring and high voltage equal to -900V shows a slightly worse time resolution, as expected.

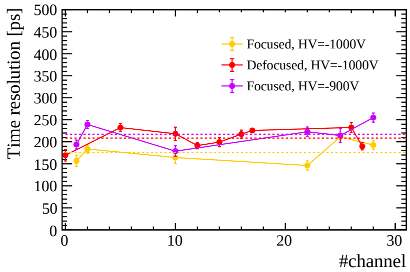

Figure 7: Time resolutions as a function of the channel number. The dotted lines represent the datasets simple mean.

Data taking conditions	σ_t (ring ch.) [ps]	σ_t (no border ch.) [ps]
Focused ring, HV=-1000V	212 ± 73	176 ± 24
Defocused ring, HV=-1000V	234 ± 84	208 ± 22
Focused ring, HV=-900V	229 ± 37	217 ± 29

Table 1: Average time resolution results for different beam test data taking conditions.

7. Conclusions

In these proceedings the first time resolution results for the prototype readout chain with picosecond timing capabilities for the LHCb RICH detector upgrades has been presented. Such prototype, including the FastIC, has been extensively tested in a beam test campaign at CERN-SPS. The results are promising and the 1-inch MAPMT time resolution estimation is compatible with the expected Transit Time Spread. These results give a strong basis to pursue the studies for the next LHCb RICH upgrades.

References

[1] Bartolini, M. and others, *LHCb RICH Fast-timing photon detector studies at the SPS charged particle beam*, LHCb-DP-2023-004, 2023.

[2] F. Keizer, *Sub-nanosecond Cherenkov photon detection for LHCb particle identification in high-occupancy conditions and semiconductor tracking for muon scattering tomography*, CERN-THESIS-2019-203, 2020, 10.17863/CAM.45822.

[3] LHCb Collaboration, *LHCb Particle Identification Enhancement Technical Design Report*, CERN-LHCC-2023-005, 2023.

[4] Gómez, S. and others, *FastIC: a fast integrated circuit for the readout of high performance detectors*, JINST 17 05 C05027, 2022, 10.1088/1748-0221/17/05/C05027.

[5] L.N. Cojocariu and D. Foulds-Holt and F. Keizer and V.M. Placinta and S. Wotton, *A multi-channel TDC-in- FPGA with 150 ps bins for time-resolved readout of Cherenkov photons*, NIMA 1055 168483, 2022, 10.1016/j.nima.2023.168483 .

[6] Particle Data Group et al., *Review of Particle Physics*, Progress of Theoretical and Experimental Physics 2022 8 083C01, 2022, 10.1093/ptep/ptac097.

PoS(EPS-HEP2023)563